7000 *Biochemistry* **2010,** *49,* 7000–7011
DOI: 10.1021/bi100463d

BIOCHEMISTRY
including biophysical chemistry & molecular biology
Article

Functional and Structural Characterization of the 2/2 Hemoglobin from *Synechococcus* sp. PCC 7002[†,‡]

Nancy L. Scott,[§,△] Yu Xu,[∥,△] Gaozhong Shen,[∥] David A. Vuletich,[§,◇] Christopher J. Falzone,[⊥] Zhongkui Li,[∥] Marcus Ludwig,[∥] Matthew P. Pond,[#] Matthew R. Preimesberger,[#] Donald A. Bryant,*[,∥] and Juliette T. J. Lecomte*[,#]

[§]*Department of Chemistry,* [∥]*Department of Biochemistry and Molecular Biology, The Pennsylvania State University, University Park, Pennsylvania 16802,* [⊥]*Department of Chemistry, and* [#]*T. C. Jenkins Department of Biophysics, Johns Hopkins University, Baltimore, Maryland 21218.* [△]*N.L.S. and Y.X. contributed equally.* [◇]*Current address: Department of Chemistry, The College at Brockport, SUNY, Brockport, NY 14420.*

Received March 28, 2010; Revised Manuscript Received July 18, 2010

ABSTRACT: Cyanobacterium *Synechococcus* sp. PCC 7002 contains a single gene (*glbN*) coding for GlbN, a protein of the 2/2 hemoglobin lineage. The precise function of GlbN is not known, but comparison to similar 2/2 hemoglobins suggests that reversible dioxygen binding is not its main activity. In this report, the results of in vitro and in vivo experiments probing the role of GlbN are presented. Transcription profiling indicated that *glbN* is not strongly regulated under any of a large number of growth conditions and that the gene is probably constitutively expressed. High levels of nitrate, used as the sole source of nitrogen, and exposure to nitric oxide were tolerated better by the wild-type strain than a *glbN* null mutant, whereas overproduction of GlbN in the null mutant background restored the wild-type growth. The cellular contents of reactive oxygen/nitrogen species were elevated in the null mutant under all conditions and were highest under NO challenge or in the presence of high nitrate concentrations. GlbN overproduction attenuated these contents significantly under the latter conditions. The analysis of cell extracts revealed that the heme of GlbN was covalently bound to overproduced GlbN apoprotein in cells grown under microoxic conditions. A peroxidase assay showed that purified GlbN does not possess significant hydrogen peroxidase activity. It was concluded that GlbN protects cells from reactive nitrogen species that could be encountered naturally during growth on nitrate or under denitrifying conditions. The solution structure of covalently modified GlbN was determined and used to rationalize some of its chemical properties.

The hemoglobin (Hb)[1] superfamily consists of proteins from three phylogenetically distinct lineages (*1*). Two of these lineages are represented by proteins with the well-known α-helical structure of sperm whale myoglobin and referred to as a 3/3 orthogonal bundle. The third Hb lineage, which was discovered in bacteria, archaea, unicellular eukaryotes, and plants, comprises the "truncated" Hbs, proteins displaying a 2/2 orthogonal bundle topology (*2*). Further phylogenetic analyses divide the 2/2 Hbs into three groups (I, II, and III), each showing specific patterns of residue conservation (*3*). Although the number of deposited 2/2 Hb sequences has grown rapidly over the past decade, limited functional information is currently available for these proteins. Nevertheless, the data already support that the versatile 2/2 fold is capable of tuning heme reactivity to achieve physiological tasks other than the reversible dioxygen binding exhibited by 3/3 Hbs (*4*), including dioxygen scavenging, nitric oxide processing, protection against oxidative damage, and recently sulfide binding (*5*).

The cyanobacterium *Synechococcus* sp. strain PCC 7002 (henceforth *Synechococcus* 7002) is an organism that possesses a gene (*glbN*) encoding a Group I 2/2 Hb (*6*). In prior work, the corresponding protein (GlbN) was produced heterologously in *Escherichia coli* (*6*). Recombinant GlbN contains 123 residues after cleavage of the initial Met, binds a single heme group, and is monomeric. In its purified form, this cyanobacterial Hb exhibits two rare structural properties: it has *bis*-histidyl coordination of the heme iron in the absence of an exogenous ligand (*6*), and it undergoes a facile, post-translational covalent attachment of the *b* heme to the globin by modification of the 2-vinyl substituent (*7*). Despite *bis*-histidine coordination, *Synechococcus* 7002 GlbN is capable of exogenous ligand binding, which it accomplishes by displacing the distal histidine (His46, or E10) from the iron (*6*, *8*). To date, the function of this protein and its relationship to the metabolism of dioxygen, nitric oxide, or various reactive nitrogen and oxygen species are unknown.

Two other cyanobacterial Group I 2/2 Hbs have been partially characterized. The protein most closely related to *Synechococcus* 7002 GlbN occurs in *Synechocystis* sp. strain PCC 6803 (henceforth *Synechocystis* 6803). *Synechocystis* 6803 GlbN is 59%

[†]This study was supported by National Science Foundation Grants MCB-0519743 (D.A.B.), MCB-0349409 (J.T.J.L.), and MCB-0843439 (J.T.J.L.), Air Force Office of Sponsored Research Grant FA9550-05-1-0365 (D.A.B.), and NASA Fellowship NNG04GN33H (D.A.V.).

[‡]Coordinates have been deposited in the Protein Data Bank (PDB) as entry 2KSC.

*To whom correspondence should be addressed. D.A.B.: tel, (814) 865-1992; fax, (814) 863-7024; e-mail, dab14@psu.edu. J.T.J.L.: tel, (410) 516-7019; fax, (410) 516-4118; e-mail, lecomte_jtj@jhu.edu.

[1]Abbreviations: CAB, chlorophyll *a*/*b* binding; Hb, hemoglobin; HLIP, high-light-induced protein; LB, Luria−Bertani; PS, photosystem; rGlbN-R, recombinant GlbN reconstituted with heme; rGlbN-A, recombinant GlbN with covalently attached heme; RNS, reactive nitrogen species; ROS, reactive oxygen species; *Synechococcus* 7002, *Synechococcus* sp. PCC 7002; *Synechocystis* 6803, *Synechocystis* sp. PCC 6803.

 Published on Web 07/19/2010

identical in sequence to *Synechococcus* 7002 GlbN and shares the features of *bis*-histidine heme coordination (*9*, *10*) and heme covalent attachment (*7*). Other properties, e.g., the rate of cyanide binding to ferric heme (*8*) and the apoprotein thermodynamic stability (*11*), differ significantly. To our knowledge, no physiological data are available for *Synechocystis* 6803 GlbN, and the function of this protein has not been determined. The second partially characterized cyanobacterial GlbN occurs in *Nostoc commune* UTEX 584 (*12*). Sequence identity of this protein with *Synechococcus* 7002 GlbN is low (30%), *bis*-histidine coordination is not systematically observed (*13*, *14*), and according to the primary structure, the covalent heme−protein linkage found in *Synechococcus* 7002 GlbN and *Synechocystis* 6803 GlbN cannot form. Because of the localization of *N. commune* GlbN in heterocysts, the function of the protein has been related to nitrogen fixation, likely as an oxygen scavenger (*15*). The inability of *Synechococcus* 7002 and *Synechocystis* 6803 to fix nitrogen and the distinct chemical properties of their GlbNs support the necessity of in vivo and in vitro investigations to establish robust structure−function relationships in these enigmatic cyanobacterial Hbs.

Here we report the results of physiological studies that were conducted with *Synechococcus* 7002 to delineate the role of GlbN in its native context. A set of fundamental questions were considered, which included the transcriptional regulation of the *glbN* gene, the phenotypes associated with a *glbN* null mutant, the effects of GlbN overproduction, and the state of the protein product in the cyanobacterial cell. To assess functional hypotheses, the structure of *Synechococcus* 7002 GlbN in the *bis*-histidine ferric state with covalently attached heme was determined in solution by NMR methods. The physiological results and the newly determined structure allow one to infer the properties of related cyanobacterial Hbs.

MATERIALS AND METHODS

Cell Culture and Growth Measurement of Cyanobacteria. *Synechococcus* 7002 wild-type and mutant strains were grown at 38 °C in liquid medium A containing 12 mM nitrate (medium A^+) (*16*) under constant cool-white fluorescent illumination at an intensity of 250 μmol of photons m^{-2} s^{-1} while sparging with air supplemented with 1% (v/v) CO_2 (designated as standard (oxic) conditions) or with 99% N_2 containing 1% (v/v) CO_2 (microoxic conditions). Additional details concerning growth conditions to probe GlbN function and for transcriptional analyses are described in the Supporting Information.

Measurement of Cellular Reactive Oxygen/Nitrogen Species (ROS/RNS) Content. The cytosolic ROS/RNS content of live cyanobacterial cells was estimated using the membrane-permeant reactive oxidation-activated fluorophor 5- (and 6-) chloromethyl-2′,7′-dichlorodihydrofluorescein diacetate, acetyl ester (CM-H_2DCFDA) from Invitrogen Molecular Probes (Eugene, OR). The protocol recommended by the manufacturer was followed. In addition to ROS such as hydrogen peroxide, peroxyl radicals, and hydroxyl radicals, CM-H_2DCFDA also detects peroxynitrite ions but not nitric oxide.

Construction of the glbN Mutant. For PCR-based generation of the *Synechococcus* 7002 *glbN* deletion mutant, a 520-bp DNA fragment (glbN5U) from the upstream region of the *glbN* gene was amplified by PCR using the primers 1glbNUPF (5′GTTGATCTGTCCGACGTC-GAG3′) and 2glbNUPR (5′TTCATTCATCGTCGACACCAAAACC3′), and a 530-bp DNA fragment glbN3D from the region downstream from the *glbN* gene was amplified by PCR using the primers 3glbNDNF (5′GTCGTTAGTCTGCAGCGACCATTGCACAG3′) and 4glbNDNR (5′CATCCCTATAGTTAATCGAACGATATC3′). After the glbN5U fragment was digested with *Sal*I and the glbN3D fragment was digested with *Pst*I, these DNA fragments were ligated to a 1-kb spectinomycin-resistance cartridge (*aadA*), which had *Sal*I and *Pst*I sites at its 5′ and 3′ ends, respectively. The resulting ligation product was directly used to transform *Synechococcus* 7002 cells. Transformants were screened on medium A^+ plates containing spectinomycin (200 μg mL^{-1}). Complete segregation of the *glbN* and Δ*glbN::aadA* alleles was confirmed by PCR analysis using primers 1glbNUPF and 4glbNDNR.

Generation of the glbN Expression Construct. For expression of [His_{10}]-tagged *Synechococcus* 7002 GlbN, the *glbN* gene was cloned into either plasmid pAQ1Ex*::P_{aphII}* that includes the *aphII* promoter from Tn5 or plasmid pAQ1Ex*::P_{cpcBA}* that includes the *cpcBA* promoter for the *cpcBA* operon of *Synechocystis* 6803 (*17*). A 400-bp DNA fragment containing the *glbN* gene was amplified through PCR using the primers GlbnN1F (5′GGAGATTCGCATATGGCTAGTTTGTATG3′) and GlbnB1R (5′ATCGATACTGGATCCTAACGGTTTAAAAC3′). The PCR product was purified, digested with *Nde*I and *Bam*HI, and cloned into the *Nde*I and *Bam*HI sites of pAQ1Ex-P_{aphII} to produce the expression plasmid pAQ1Ex*::P_{aphII}::glbN* and into plasmid pAQ1Ex*::P_{cpcBA}* to produce plasmid pAQ1Ex*::P_{cpcBA}::glbN* (*17*). In either case the recombinant GlbN protein could be produced with an N-terminal [His_{10}] tag. For complementation of the Δ*glbN* mutant, plasmid pAQ1Ex*::P_{aphII}::glbN* (carrying the gentamycin-resistance marker, *aacCI*) was used to transform the Δ*glbN::aadA* mutant strain of *Synechococcus* 7002. Transformants were selected for resistance to both gentamycin and spectinomycin, and one of these was verified and designated as the Δ*glbN* (pAQ1Ex*::P_{aphII}::glbN*) strain of *Synechococcus* 7002. For overproduction of [His_{10}]-GlbN in *Synechococcus* 7002, *Synechococcus* 7002 wild-type cells were transformed with plasmid pAQ1Ex*::P_{cpcBA}::glbN* by selecting for spectinomycin resistance. For additional control experiments, *E. coli* cells were transformed with the pAQ1Ex*::P_{aphII}::glbN* plasmid.

DNA Isolation and RNA Purification. The isolation of chromosomal DNA from wild-type and mutant strains of *Synechococcus* 7002 was performed as previously described (*18*). Total RNA was extracted from cells harvested from liquid cultures by using the High Pure RNA isolation kit from Roche (Indianapolis, IN) essentially as described by the manufacturer. The procedure was modified to include the use of a bead beater and glass beads to disrupt cells (*18*). Isolated RNA samples were incubated with RNase-free DNase I for 1 h at room temperature to remove contaminating DNA, and the absence of contaminating DNA in the total RNA fractions was verified by PCR. RNA concentrations were determined using a NanoDrop ND-100 spectrophotometer (Thermo Scientific, Waltham, MA). A Qubit fluorometer was also used with the Quant-iT RNA assay kit to determine RNA concentrations and with the Quant-iT dsDNA assay kit to determine whether the RNA preparations contained contaminating DNA (Invitrogen Molecular Probes, Eugene, OR).

Transcriptomics Analysis. For transcription profiling, total RNA isolated from cyanobacterial cells was further purified using MICROB*Express* mRNA purification kits and MEGAclear kits from Ambion Inc. (Austin, TX). cDNA libraries were synthesized and sequenced using a SOLiD 3 Plus system

(Applied Biosystems, Foster City, CA) at the Genomics Core Facility, Huck Institutes of the Life Sciences, The Pennsylvania State University. The obtained sequences were mapped against the *Synechococcus* 7002 genome using the Burrows−Wheeler alignment tool with four mismatches allowed (*19*). The aligned cDNA sequences mapping in protein-coding open reading frames were counted, and the relative transcript abundance was calculated as the number of uniquely mapped sequences for each open reading frame divided by the total number of uniquely mapped sequences within protein-coding open reading frames. For the "standard" (optimum growth condition, harvested at OD 0.7) sample, data sets were obtained for three biological replicates, and mean values were calculated and used as the basis for all subsequent comparisons. The relative transcript abundance obtained under different growth conditions was compared [as a ratio of relative abundance under condition 2 divided by relative abundance under condition 1 (standard/optimum growth condition)]. The change in the transcript level was calculated in fold standard deviation to estimate the probability that these genes were differentially transcribed.

SDS−PAGE, Immunoblotting, and Heme Staining. Methods used for polyacrylamide gel electrophoresis in the presence of sodium dodecyl sulfate (SDS−PAGE) and immunoblotting were identical to those previously described (*20*). For monitoring the expression of [His_{10}]-tagged GlbN, *Synechococcus* 7002 cells harboring pAQ1Ex*::*P_{aphII}*::glbN* were grown under different conditions (i.e., standard and microoxic conditions), were harvested, and were lysed either by using BugBuster protein extraction reagent from Novagen (Madison, WI) or by passing the cells through a chilled French pressure cell three times at 138 MPa. Clarified cell extracts resulting from both lysis approaches were subjected to SDS−PAGE and immunoblotting analyses or were used for small-scale purification of recombinant [His_{10}]-GlbN protein through a Ni-NTA affinity chromatography (Novagen). [His_{10}]-tagged GlbN was detected immunologically with anti-6×-His EPITOPE TAG antibodies from Rockland Immunochemicals (Gilbertsville, PA). To determine whether GlbN contained a covalently attached heme group, the purified protein was subjected to SDS−PAGE, and heme staining of gels (or membranes) was performed using 3,3′,5,5′-tetramethylbenzidine as described (*21*). The same detection procedures were applied to the overproduced protein obtained by transformation of *E. coli* cells expressing the *glbN* gene from the plasmids used to transform *Synechococcus* 7002.

Overproduction and Purification of GlbN. For NMR characterization, GlbN was prepared without a His tag as previously reported (*6*, *11*) and summarized in the Supporting Information. To specify the nature of the samples and how they were obtained, the heterologously expressed, recombinant protein with an unmodified *b* heme is referred to as rGlbN-R (recombinant GlbN Reconstituted with *b* heme, also referred to as rHb-R in previous work); by analogy, -R designates a protein containing a *b* heme. The protein with the heme−protein cross-link (hybrid *b*/*c* heme) is designated with -A for Adduct. Heme structure and the nomenclature employed are shown in Supporting Information Figure S1.

Electronic absorption spectra were collected at 25 °C on an Aviv model 14 DS spectrophotometer. Holoprotein concentrations are reported on the basis of heme content using ε_{411nm} = 96 mM^{-1} cm^{-1} for rGlbN-R and ε_{409nm} = 87 mM^{-1} cm^{-1} for rGlbN-A (*11*). The $A_{Soret\ max}$-to-$A_{280\ nm}$ ratio was approximately 5.4 for the pure ferric proteins.

rGlbN Peroxidase Assays. The peroxidase activity of ferric rGlbN-R and rGlbN-A was evaluated spectroscopically using guaiacol (>98%, Sigma-Aldrich) as the electron donor (*22*). Guaiacol and H_2O_2 (30%, Fisher) solutions were prepared the day of their use, and their concentration was evaluated with ε_{274nm} = 2.55 mM^{-1} cm^{-1} and ε_{240nm} = 39.4 mM^{-1} cm^{-1}, respectively. Absorption was measured at room temperature on a Varian Cary 50 series spectrophotometer. Reaction solutions contained 1.3 μM (rGlbN-R) or 2.1 μM (rGlbN-A) purified protein (10 mM guaiacol, ~100 mM phosphate buffer, pH 7.30) and were incubated at least 5 min prior to reaction initiation by addition of H_2O_2. Additional runs at lower and higher rGlbN concentration and with cyanide present were also performed. Peroxidase activity was determined by monitoring product concentration (A_{470nm}) as a function of time using ε_{470nm} = 26.6 mM^{-1} cm^{-1}. Michaelis−Menten parameters were obtained by measuring the initial rates of tetraguaiacol formation as a function of H_2O_2 concentration (4−140 mM). Catalytic parameters (k_{cat} and K_M) were extracted from the data by nonlinear least-squares fitting (Kaleidagraph, Synergy Software). Each data point represents the average of three measurements. The parameters and susceptibility of the heme to damage were such that steady-state kinetics at constant H_2O_2 concentration and variable guaiacol concentration were not performed.

NMR Spectroscopy. ^1H, ^{13}C, and ^{15}N protein assignments and ^1H and ^{13}C heme assignments have been reported (*6*, *7*, *11*, *23*). $^3J_{H\alpha\text{-}HN}$ values were determined with HNHA data (*24*). Spectra were processed with NMRPipe (*25*) and analyzed with SPARKY (*26*).

The apparent pK_a of His117 in rGlbN-R was obtained with a 700 μM protein sample in ^2H_2O. The pH* (uncorrected for isotope effects) was adjusted between 9.4 and 4.7 by addition of NaO^{2}H or ^{2}HCl (0.1 or 1.0 M titrant). The chemical shifts of CδH and CεH were compiled as a function of pH* and analyzed with a modified Henderson−Hasselbalch equation appropriate for fast exchange (on the chemical shift time scale) between protonated and neutral states (*27*).

Structure Calculations. Distance restraints were derived from four main NMR data sets at pH 7.2: homonuclear NOESY in ^2H_2O and ^1H_2O, ^{15}N-separated NOESY, and ^{13}C-separated NOESY. H-exchange data (*11*) were used to generate H-bond restraints. Only the amide hydrogens maintaining an intensity larger than 20% of their original value after 14 min of exchange at pH 7.4 were used. The acceptors were identified with UCSF Chimera (*28*) (default parameters) and adjusted iteratively as the structures were refined. Capping (side-chain:main-chain) interactions were inferred from these structures and chemical shift in the case of Thr80 NH−His83 Nδ1. Backbone dihedral angles φ and ψ were evaluated using TALOS+ (*29*). Side-chain χ_n angles were determined using $^3J_{\alpha\beta}$ coupling constants (χ_1) and NOE magnitudes. Distance categories and additional details are provided in the Supporting Information.

X-PLOR-NIH 2.19.1 (*30*) was used with standard protein topology and parameter files (protein.top and protein.par, respectively) without adjustments. Histidine residues were patched to account for their tautomeric state as determined experimentally with $^1H-^{15}N$ HMQC data. The topology file for the modified heme group (*7*) was constructed from standard heme and histidine topologies. The porphyrin ring was made planar, and the NE2−CAB bond distance (His117 Nε2 to Cα on pyrrole B) was set to 1.479 Å (*31*). Bond angles were set to sp^3 values at the Cα and sp^2 values at the Nε2. The *R* stereochemistry

at CAB (*7*) was enforced in the X-PLOR template of the modified heme, which is referred to as "HEB" in the coordinate file (PDB ID 2KSC).

Axial coordination by His46 and His70 was achieved with distance restraints; the Nε2−Fe equilibrium distance was set to 2.1 Å (1.9−2.2 Å) and the Nε2−Nε2 distance to 4.2 Å (4.0−4.3 Å). This allowed the ligation bonds and angles to vary within reasonable limits. The angles formed by the projection of the imidazole planes and the heme NA−NC axis were restrained to the values derived from hyperfine chemical shift analysis (*7*). As a consequence of the various geometry assumptions, details such as heme doming and inclination of the axial histidines with respect to heme normal were not captured by the model, which is best used in the comparison of different forms of the wild-type and variant proteins.

Structures were calculated with a distance geometry/simulated annealing protocol and refined with a Gaussian DELPHIC torsional potential to improve the Ramachandran plot and the rotamer distribution (*32*) as described for *Synechocystis* 6803 rGlbN-R (*33*). The resulting family of structures was evaluated with PROCHECK (*34*) and WHATCHECK (*35*). Tunnels were detected with MOLE (*36*) using as starting point the Nε2 atom of His46.

To determine the local structure around His117 in ferric rGlbN-R, each NOE involving the heme group and His117 was inspected in ^{1}H spectra at pH ~7.8, a pH at which the lines are sharp. A model was constructed by using the adjusted distances in the background of the remaining rGlbN-A distance restraints. Hydrogen bond restraints were taken from H-exchange data at pH 7.4 (*11*) as described for rGlbN-A, and dihedral angles were from a TALOS+ analysis at pH 6.2 (*23*). Differences in pH did not appear to affect the structure. Small variations were expected to be accommodated within restraint boundaries.

RESULTS

Physiological Characterization of the Δ*glbN Mutant*. As shown in Supporting Information Figure S2 and verified by PCR analysis, the *glbN* and Δ*glbN::aadA* alleles segregated fully in *Synechococcus* 7002 to produce a homozygous deletion mutant, Δ*glbN*. Under standard growth conditions in replete medium, the Δ*glbN* mutant showed no obvious growth deficiency compared to wild type. However, when cells were grown under limiting Fe or CO_2, slower growth rates were measured for the Δ*glbN* mutant than for the wild type (Supporting Information Table S1). The difference in growth rate was most pronounced when cells were limited for both Fe and CO_2. A possible explanation for this behavior is that these cells experience ROS/RNS stress (see below). Using the relatively weak *aphII* promoter (*17*), expression of the *glbN* gene (modified to code for the [His_{10}]-tagged product) from plasmid pAQ1 in the Δ*glbN* background complemented the *glbN* deletion mutant and restored growth rates to values similar to those of the wild-type strain (Supporting Information Table S1).

Low-temperature fluorescence emission spectroscopy (Supporting Information Figure S3) demonstrated an effect of the combined Fe and CO_2 limitations on the assembly of the two photosynthetic reaction center complexes, photosystem I (PS I) and photosystem II (PS II). The observations were consistent with Δ*glbN* cells containing substantially lower PS I concentration than the wild-type cells grown under the same conditions. Spectral changes characteristic of those that occur when CP43′, encoded by the *isiA* gene, and small CAB-like proteins (HLIPs) are induced by Fe limitation or high-light stress (*37*, *38*) were more pronounced in Δ*glbN* cells than wild-type cells. The data supported further that the Δ*glbN* cells were experiencing enhanced stress relative to the wild type (also see below).

Mycobacterium bovis contains a Group I 2/2 Hb (trHbN) closely related to GlbN and known to protect the cell against nitric oxide damage (*39*). To investigate whether the *glbN* gene product played a similar role in the response of *Synechococcus* 7002 cells to nitrosative stress, growth recovery after spermine NONOate treatment was compared for wild-type and Δ*glbN* cells. Different concentrations of spermine NONOate were tested with the initial cell concentration held constant (OD_{730nm} = 0.1). After exposure to 0.5 mM spermine NONOate, wild-type cells hardly grew at all. However, after treatment with 0.1 mM spermine NONOate, wild-type cells slowly recovered. After treatment with 0.1 mM spermine NONOate, the Δ*glbN* mutant recovered much more slowly than the wild type but eventually grew with a doubling time only slightly slower than that of the wild type (Supporting Information Figure S4).

Nitric oxide can react with superoxide to form peroxynitrite, which is a strong oxidant (*40*). Therefore, one possible reason for the growth inhibition caused by the nitric oxide released from spermine NONOate is oxidative stress caused by an enhanced production of ROS/RNS. To test this hypothesis, cellular ROS/RNS contents were measured in control cells or in cells after treatment with spermine NONOate. In cells grown under standard conditions (replete medium, no spermine NONOate exposure), the ROS/RNS content of the Δ*glbN* cells was about 40% higher than in wild-type cells (Figure 1). When both strains were treated with spermine NONOate, this percentage rose to 75%, the ROS/RNS levels of the wild-type cells increasing about 3.5-fold and those of the Δ*glbN* cells nearly 4.5-fold (Figure 1). Notably, the ROS/RNS level in the treated Δ*glbN* cells was ~6-fold higher than that in the control. These results showed that cells lacking GlbN have much higher ROS/RNS levels than wild-type cells, and this could explain the greater sensitivity of Δ*glbN* cells to NO treatment.

The results of the NO challenge experiments directed the investigation toward nitrogen metabolism and the scavenging of RNS. Cells of the wild-type and mutant strains were grown in medium A supplemented with increasing concentrations of $NaNO_3$. The doubling times are listed in Table 1, and photographs of the cultures are shown in Supporting Information Figure S5. When the concentration of nitrate was increased from 12 to 90 mM, the wild-type strain showed no significant effect and maintained a doubling time of ~4.2 h. The Δ*glbN* cells, in contrast, grew increasingly more slowly and exhibited signs of chlorosis (Supporting Information Figure S5), an indicator of stress in cyanobacterial cells. When the nitrate concentration was raised to 240 mM, the Δ*glbN* mutant was unable to grow under oxic conditions but exhibited very slight growth under microoxic conditions, although the wild type continued to grow with doubling times of 5.8 h (oxic) and 7.3 h (microoxic). Complementation of the Δ*glbN* strain with the pAQ1Ex::P_{cpcBA}::*glbN* plasmid restored growth almost to wild-type levels under microoxic conditions (Table 1). Both strains grew slowly on a low concentration of nitrite (5 mM), whereas urea at 10 mM had practically no effect.

The ROS/RNS analyses of the cells described above were informative (Figure 1). They demonstrated that the null mutant accumulated ROS/RNS as the nitrate concentration was increased. A much smaller increase, within the error of the measurement up to 90 mM nitrate, was noted for the wild-type

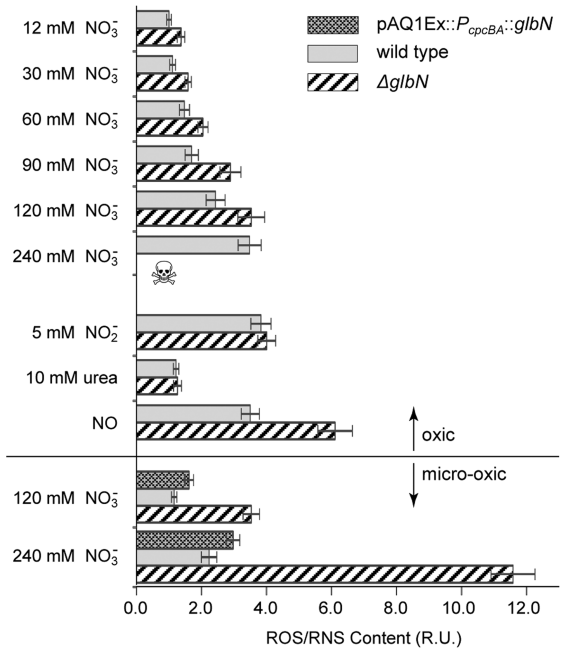

FIGURE 1: Relative ROS/RNS content of *Synechococcus* 7002 wild-type cells, Δ*glbN* mutant cells, and Δ*glbN* (pAQ1Ex*::*P_{cpcBA}*::glbN*) strain cells. The ROS/RNS content was measured after incubation under standard growth conditions (38 °C, 1% (v/v) CO_2 in air, 250 μmol of photons m^{-2} s^{-1}, $OD_{730\ nm}$ = 0.7) or microoxic conditions (38 °C, 1% (v/v) CO_2, 99% (v/v) N_2, 250 μmol of photons m^{-2} s^{-1}, $OD_{730\ nm}$ = 0.7). Relative values are with respect to the content of wild-type cells grown under standard conditions. The concentration of nitrate, nitrite, or urea complementing the A medium is specified on the left. NO indicates ROS/RNS cells incubated under standard growth conditions in the presence of 0.1 mM spermine NONOate for 4 h prior to analysis. The number for Δ*glbN* mutant cells under microoxic conditions and 240 mM nitrate was obtained by performing the measurement on pelleted cells obtained from cultures that were growing too slowly to allow a reliable determination of the growth rate. Complete growth inhibition was observed for Δ*glbN* mutant cells under oxic conditions and 240 mM nitrate.

Table 1: Comparison of the Doubling Times (h) of *Synechococcus* 7002 Wild Type and Δ*glbN* Mutant Grown with Different Nitrogen Sources or Concentrations

	wild type	Δ*glbN*	Δ*glbN* (pAQ1EX*::*P_{cpcBA}*::glbN*)[a]
12 mM $NaNO_3$[b]	4.2 ± 0.2	4.4 ± 0.2	
30 mM $NaNO_3$	4.1 ± 0.1	4.5 ± 0.2	
60 mM $NaNO_3$	4.1 ± 0.2	4.7 ± 0.3	
90 mM $NaNO_3$	4.4 ± 0.2	5.2 ± 0.2	
120 mM $NaNO_3$	4.9 ± 0.2	8.1 ± 0.2	
240 mM $NaNO_3$	5.8 ± 0.2	ng[c]	
120 mM $NaNO_3$ microoxic	5.4 ± 0.4	6.7 ± 0.6	5.9 ± 0.4
240 mM $NaNO_3$ microoxic	7.3 ± 0.3	nm[d]	9.2 ± 0.6
5 mM $NaNO_2$	6.1 ± 0.4	6.3 ± 0.3	
50 mM urea	3.7 ± 0.1	3.8 ± 0.2	

[a] Δ*glbN* mutant complemented with P_{cpcBA}*::glbN* encoded in plasmid pAQ1. [b] Medium A supplemented with the indicated concentration of nitrogen compound; conditions otherwise standard, i.e., oxic, unless otherwise noted. [c] No growth. [d] Not measured.

strain. Cells grown on a medium containing nitrite exhibited the highest levels (4-fold increase), and correspondingly these cells had the most chlorotic appearance (Figure S5A). There was no difference in ROS/RNS levels when the cells were grown on urea. When cells were grown under microoxic conditions and high nitrate concentration, elevated ROS/RNS levels were also observed in the Δ*glbN* cells, whereas the levels were similar to those of the wild type upon complementation with the pAQ1Ex*::*P_{cpcBA}*::glbN* plasmid. Under conditions for which the doubling time of Δ*glbN* cells was too slow to measure (240 mM nitrate), the ROS/RNS level obtained on these spun-down mutant cells was ~11-fold that of the wild-type cells under standard conditions. Thus, a clear connection was established between nitrate metabolism, ROS/RNS levels, and GlbN activity.

Transcription of the glbN Gene under Different Growth Conditions. The transcription level of the *glbN* gene was investigated quantitatively under different growth conditions by transcriptional profiling through cDNA sequencing. As documented in Table S2 of the Supporting Information, when cells were incubated in the dark (oxic or microoxic), grown under CO_2 limitation, on different nitrogen sources, or in standard cultures harvested at lower or higher densities, no large difference was observed in *glbN* transcript levels. When cells were subjected to various stress treatments, such as high-light stress, oxidative stress, low-temperature stress, and Fe or nitrogen limitation, relative transcript levels for the *glbN* gene were generally slightly lower than in cells grown under standard growth conditions (about 2-fold). When the cells were grown photomixotrophically on glycerol, *glbN* transcript levels were slightly lower, whereas in a culture grown photomixotrophically and then incubated in the dark, the *glbN* transcript level was similar to standard growth conditions. At maximum, a 3-fold decrease was observed for a culture grown photoautotrophically under microoxic conditions. A photomixotrophically grown culture under microoxic conditions showed an about 2-fold decrease in mRNA level. In no case was a significant increase above the transcript levels for standard conditions detected. Similar results were obtained by RT-PCR under selected conditions, including iron limitation and when cells were grown on air levels of CO_2. Consistent with all of these data, a preliminary proteomic analysis (S. Callister, M. Lipton, G. Shen, M. Ludwig, and D. A. Bryant, unpublished results) showed that GlbN was present at similar levels in the soluble protein fraction (and this fraction only) of cells grown under standard conditions and with air levels of CO_2. Collectively, the results suggested that GlbN expression was constitutive, that the protein was in the soluble fraction, and that GlbN was likely to be present at similarly low levels in *Synechococcus* 7002 cells under most growth conditions.

Characterization of GlbN in E. coli Cells. [His_{10}]-GlbN synthesis was achieved by transformation of *E. coli* strain DH5α with the pAQ1Ex*::*P_{aphII}*::glbN* plasmid. Cells were grown in LB medium and acquired a pinkish color typical of hemoprotein overproduction. After lysis, [His_{10}]-GlbN was purified by affinity chromatography using a nickel column and subjected to SDS−PAGE and heme staining. Figure 2A illustrates that the protein contained covalently bound heme. The absorption spectrum of purified GlbN, shown in Figure 2B, exhibited typical absorption bands at ~410 nm (Soret) and 550 nm. These features corresponded approximately to those observed in the spectrum of rGlbN in the ferric, *bis*-histidine state (*6*). Data collected on the liquid culture (Supporting Information Figure S6) exhibited absorption bands at ~420, 520, and 555 nm, resembling closely the spectrum of the purified ferrous *bis*-histidine protein (*6*). The same reduced state spectrum was obtained when *E. coli* BL21 cells containing the plasmid used for NMR sample preparation (no His tag) were grown in LB medium (data not shown).

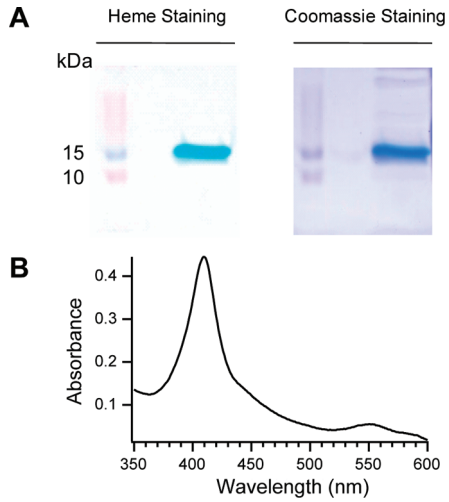

FIGURE 2: Purification and characterization of [His_{10}]-GlbN produced in *E. coli* cells. (A) [His_{10}]-GlbN was purified by Ni-chelation affinity chromatography and subjected to SDS−PAGE analysis. Gels were stained for heme (left panel) or with Coomassie Blue (right panel). (B) Absorption spectrum of purified [His_{10}]-GlbN.

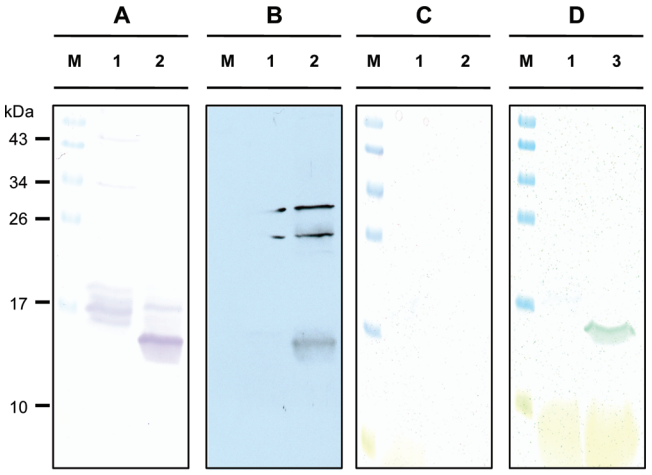

FIGURE 3: Characterization of [His_{10}]-GlbN produced in *Synechococcus* 7002. Samples were prepared from (1) the wild-type cells grown under the normal oxygenic condition, (2) the pAQ1Ex::P_{cpcBA}::*glbN* strain cells grown under the oxic conditions, and (3) the pAQ1Ex::P_{cpcBA}::*glbN* strain cells grown under the microoxic conditions in the presence of urea and with sparging by 99% (v/v) N_2 and 1% CO_2. Proteins were resolved by SDS−PAGE gel electrophoresis and detected by (A) the Coomassie Blue staining, (B) the Western blotting detection using the anti-6×-His antibody, and (C, D) the heme staining assay.

Characterization of GlbN in Synechococcus 7002 Cells. In order to overproduce [His_{10}]-GlbN, *Synechococcus* 7002 cells were transformed with linearized plasmid pAQ1Ex::P_{cpcBA}::*glbN*. When these cells were grown under standard conditions, i.e., in the light under fully oxic conditions produced by sparging the culture with air supplemented with 1% (v/v) CO_2, [His_{10}]-GlbN was overproduced (Figure 3A,B, lane 2). Cell lysis with BugBuster yielded protein that tested negatively for covalently attached heme (Figure 3C). In fact, the electronic absorption spectrum of the folded material collected from the Ni-chelation column demonstrated only very low levels of heme. However, when cells were lysed with a French pressure cell, the electronic absorption spectrum of the purified protein indicated the presence of some heme associated with the protein (A_{410}/A_{280} ratio of ~3), a fraction of which was covalently attached according to denaturing gels stained for its presence. Because cross-linking may occur readily (*7*) and, as far as can be determined, is irreversible, it was concluded that the method of lysis altered the state of the protein, the French press promoting the formation of the cross-link and BugBuster extracting noncovalently attached heme. The combined results supported that cells grown under oxic conditions produced GlbN that contained *b* heme. The level of heme incorporation appeared to be substoichiometric, although *b* heme loss during the French press procedure could not be ruled out.

In contrast, when the cells were grown under microoxic conditions by sparging the cultures with 99% nitrogen and 1% (v/v) CO_2, heme staining showed that the extracted [His_{10}]-GlbN polypeptide carried covalently bound heme (Figure 3D, lane 3) regardless of the cell lysis method employed (data not shown). The optical spectrum of the protein released with BugBuster and purified by metal affinity chromatography matched well that shown in Figure 2B (A_{410}/A_{280} ratio of ~5) and corresponded to the ferric *bis*-histidine state. The amount of isolated protein was not sufficient for structural determination, and it was assumed that the heme−protein linkage was identical to that previously detected in vitro (*6*, *7*).

The response to NO exposure observed with the wild type and Δ*glbN* mutant suggested that overproduction of GlbN might convey added resistance to nitrosative stress. To test this, the pAQ1Ex::P_{cpcBA}::*glbN* cells were grown under standard oxic and microoxic conditions and exposed to 0.1 mM spermine NONOate. The strain overproducing [His_{10}]-GlbN grew a little more slowly than the wild-type strain, but was less susceptible to inhibition by NO. Specifically, the lag phase in recovery from NO treatment was nearly eliminated, and only slightly diminished growth rates were noted compared to control cultures (Figure 4). Growth rates were equally affected under microoxic conditions and under an air level of oxygen.

Structural Determination. The ease with which the heme−protein cross-link is formed in vitro (*6*) and the observation of cross-linked protein in the preparation of GlbN from the cyanobacterial cells confirmed that the structure of rGlbN-A (prepared from apoprotein heterologously produced in *E. coli*) would be useful to inform structural hypotheses concerning its physiological roles. NMR data yielding distances and dihedral angles were therefore collected. A family of 15 structures resulting from this effort is shown in Figure 5A, and statistics are presented in Table 2.

Secondary Structure. Synechococcus 7002 rGlbN-A contains seven helices accounting for 77% of the protein in agreement with the estimate obtained from far-UV circular dichroism data (*11*). All helices are well ordered locally. Deviations from ideal α geometry are encountered in the C helix, which is a short 3_{10} element starting with a conserved N-cap, the F helix at the level of the proximal histidine (His70), and the H helix, which is interrupted between Val112 and Val115 with a proline-less kink. The EF loop (residues 59−65) is disordered and fluctuates on a time scale inappropriate for NMR detection at neutral pH (*11*). This region of the protein contained the majority of disallowed φ,ψ pairs in the Ramachandran map.

Although the A helix is formed from residue 4 to residue 8, few long-range NOEs fasten it to the rest of the protein. In X-ray structures of GlbNs and GlbN-like proteins (of which there are a dozen, carrying various ligands or amino acid replacements), Gly9 has φ,ψ dihedral angles of (113° ± 10°, 18° ± 13°). Gly9 of *Synechococcus* 7002 rGlbN-A occurs in the same region of the

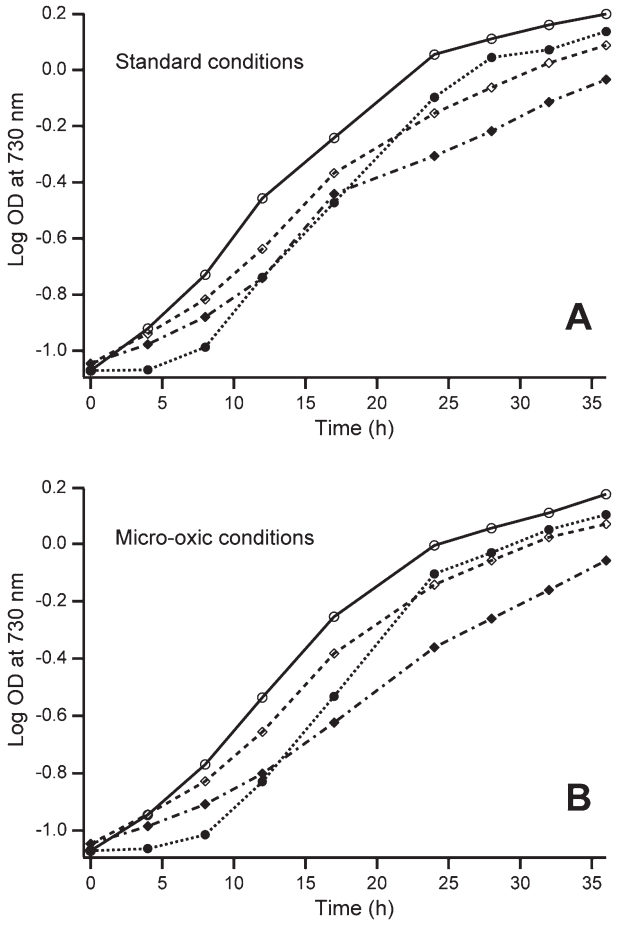

FIGURE 4: Growth curves showing the recovery of *Synechococcus* 7002 wild type and a strain overproducing [His_{10}]-GlbN (transformed with pAQ1Ex*::*P_{cpcBA}*::glbN*) after treatment with spermine NONOate. Cells were grown under standard conditions (A) or microoxic conditions (sparging with 99% N_2 and 1% (v/v) CO_2) (B). Growth was compared for untreated wild-type cells (○), wild-type cells treated with spermine NONOate (●), untreated cells overproducing [His_{10}]-GlbN (transformed with pAQ1Ex*::*P_{cpcBA}*::glbN*) (◇), and cells overproducing [His_{10}]-GlbN (transformed with pAQ1Ex*::*P_{cpcBA}*::glbN*) after treatment with spermine NONOate (◆). Cells ($OD_{730\ nm}$ = 0.1) were treated with 0.1 mM spermine NONOate at time zero, and growth was monitored for 36 h. The logarithm of $OD_{730\ nm}$ is plotted as a function of time. Data are derived from a single growth experiment, but consistent results were obtained from three independent experiments.

Ramachandran map. In contrast, Gly10 exhibits disallowed values centered at (−160° ± 10°, 110° ± 13°), whereas X-ray structures show values of (79° ± 10°, −162° ± 13°). It is interesting that the TALOS+ library (*29*) does not contain good matches for Gly10. We interpret its calculated dihedral angles to reflect local conformational fluctuation and propose that Gly10 is the hinge connecting the A and B helices. Likewise, only Gly56 in the Gly56-Gly57 turn terminating the E helix has acceptable backbone dihedral angles in agreement with X-ray structures. The Gly57 φ,ψ pair is disallowed, and the chemical shifts yield ambiguous TALOS+ results. Other ambiguous regions encompass the Asn76-Ala77-Gly78 insertion at the end of the F helix and the Gly113-Ser114 pair. Because of these flexible stretches, neither an individual structure nor the ensemble average is likely to offer a faithful representation of the molecule in solution. The NMR model has other shortcomings, for example, in the description of Arg and Lys side chains for which restraints are few.

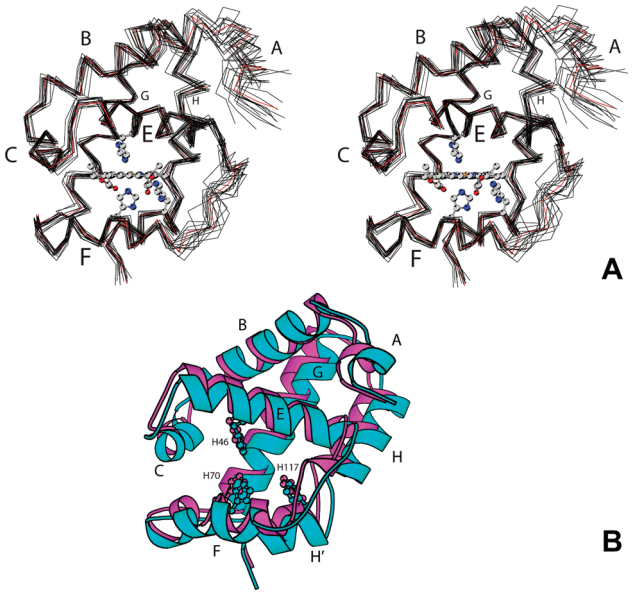

FIGURE 5: (A) Stereoview of 15 Cα traces calculated for ferric *Synechococcus* 7002 rGlbN-A (PDB ID 2KSC). The minimized average structure is shown in red as a 16th trace. The displayed heme group, axial His46 and His70, and His117 belong to this structure. The residues involved in the seven helices are as follows: A helix (4−8), B helix (12−27), C helix (29−37), E helix (40−55), F helix (66−77), G helix (81−98), and H helix (102−112 and 115−122, denoted H′ in the figure). The structures were aligned using the N−Cα−C atoms of residues 17−26, 29−33, 41−54, 67−75, 83−97, 102−112, and 116−122. (B) Overlay of the ribbon diagram of ferric *Synechocystis* 6803 rGlbN-A (1RTX) and ferric *Synechococcus* 7002 rGlbN-A (minimized average, this work). The orientation is the same as in (A). His46, His70, and His117 are shown. The modified heme is omitted for clarity.

Table 2: Restraints and Structural Statistics for Structure 2KSC

restraints	
intraresidue NOEs	379
medium-range NOEs (residue *i* to *i* + 2, 3, 4)	575
long-range NOEs (residue *i* to *i* + *n*, *n* = >5)	351
hydrogen bonds	112
dihedral angle restraints (φ, ψ, χ)	341
total structural restraints	1758
structural statistics	
rmsd for backbone atoms (fit)	0.475
rmsd for backbone atoms (all)	1.131
rmsd for side chain atoms (all)	1.515
rmsd for side chain atoms (fit)	0.650
rmsd for all atoms	1.568
average number of distance violations (per structure)	19 ± 4
number of distance violations >0.1 Å	0
average number of dihedral angle violations >2° (per structure)	6 ± 1
number of dihedral angle violations >5°	0
residues in most favored regions of Ramachandran plot (%)	94.4
residues in additional allowed regions of Ramachandran plot (%)	4.5
residues in generously allowed regions of Ramachandran plot (%)	0.8
residues in disallowed regions of Ramachandran plot (%)	0.2
rmsd for covalent bonds (Å)	0.00116 ± 0.00006
rmsd for covalent angles (deg)	0.362 ± 0.006
rmsd for improper angles (deg)	0.199 ± 0.007

Fold and Heme Pocket. The supersecondary structure of *Synechococcus* 7002 rGlbN-A is characteristic of Group I 2/2

Hbs (*2*). The 2/2 orthogonal bundle is composed of the B and E helices and the G and H helices. The heme pocket is formed by portions of the C, E, F, G, and H helices. Aside from His46, His70, and His117, several residues have one or more atoms within 4 Å from the prosthetic group: Val31 and Phe34 (C helix); Phe35 and Thr38 (CD loop); Ala49, Phe50, and Tyr53 (E helix); Phe61 (EF loop); Met66, Ala69, and Leu73 (F helix); Leu79 (FG turn); Phe84 and Ile87 (G helix); and Val112 and Val121 in the H helix. This last residue is close to the iron because of a bend in the H helix, which in rGlbN-R also brings His117 near the heme 2-vinyl substituent. Other essential residues in the heme pocket of Group I 2/2 globins include those that form hydrogen bond networks in the presence of exogenous ligand (*41*): Tyr22 (B10), Gln43 (E7), and Gln47 (E11). In the *bis*-histidine complex, these residues point away from the heme iron.

Structural Comparison to Synechocystis 6803 GlbN. Figure 5B shows the superimposition of the *Synechococcus* 7002 rGlbN-A minimized average structure and the X-ray structure of ferric *Synechocystis* 6803 rGlbN-A (PDB ID 1RTX (*42*)). The rmsd was ~1.2 Å, calculated over the ordered regions of *Synechococcus* 7002 rGlbN-A (107 Cα pairs out of 123). The largest deviations were found in the A helix and EF region. Differences in the heme pocket were also caused by the parameters used for the covalent linkage in the NMR structure, as the CAB−NE2 distance is ~0.5 Å longer in the X-ray structure than set in the X-PLOR template.

Synechococcus 7002 and *Synechocystis* 6803 rGlbN-As achieve the same helical topology with variations in two helix-breaking motifs, one at the beginning of the H helix in the sharp GH turn, the other after four turns of the helix. The H helix of *Synechocystis* 6803 rGlbN-A starts with Glu102. Pro101 has backbone dihedral angles in the PP_{II} region of the Ramachandran map and acts as the Ncap. The motif resembles an N-capping box with N′−N3/N4 (Val100−Leu104/Ile105) interactions. *Synechococcus* 7002 rGlbN-A has a serine at the Ncap position. The dihedral angles, including those of Val100, conform to those of the N′−N4 capping box, and the Oγ atom of Ser101 appears positioned to serve as the H-bond acceptor for the backbone NH of Asp103. Multiple sequence alignments of Group I 2/2 Hbs show that the Ncap position is preferentially occupied by Pro and Ser and suggest that the tight turn geometry is preserved across these proteins.

Both *Synechococcus* 7002 rGlbN-A and *Synechocystis* 6803 rGlbN-A have a long EF loop that displays exchange broadening and gives rise to few NOEs. At pH 7.2, only the ring protons of Phe61 are clearly detected in the Asp59−Ser65 stretch of *Synechococcus* 7002 rGlbN-A. In *Synechocystis* 6803 rGlbN-A protein, Tyr65 forms a hydrogen bond with the heme 7-propionate (Supporting Information Figure S7), and Tyr61 and Met66 are in contact with the heme 1- and 8-methyls. In *Synechococcus* 7002 GlbN, the Tyr61Phe and Tyr65Ser replacements are expected to alter protein−heme interactions and may be responsible for the difference in observed rates of cyanide binding between the two GlbNs (*8*).

Many Group I 2/2 Hbs have distinctive cavities and tunnels connecting the distal side of the heme to the solvent (*43*) and facilitating substrate diffusion and storage (*44*). Analysis of the *Synechococcus* 7002 rGlbN-A structure with the program MOLE (*36*) predicted distal side accessibility near the A and D pyrroles (Supporting Information Figure S8). At neutral pH, a probe can also escape the distal side of most calculated *Synechococcus* 7002 rGlbN-A models via an opening between the mobile EF loop and the H-helix kink. This path is constricted near the heme and depends on loop conformation. Similar features are observed in *bis*-histidine *Synechocystis* 6803 rGlbN-A, but interestingly, longer and wider tunnels are formed when the distal histidine is displaced by an exogenous ligand (*45*). The same is expected of *Synechococcus* 7002 rGlbN-A, with *bis*-histidine coordination blocking access to the heme and release of the distal histidine ligation allowing a second substrate molecule to enter the active site.

Gly113 introduces a bend in the H helix of *Synechocystis* 6803 and *Synechococcus* 7002 rGlbN-As. Superimposition of the H helices of *Chlamydomonas eugametos* Hb and *Synechococcus* 7002 rGlbN-A provides evidence that, in the latter, Val115 and Gln116 can be considered as insertions. Interestingly, all Group I structures so far solved contain a similar bend near position 114, which causes the C-terminal portion of the H helix to make contact with the heme group using a β-branched aliphatic residue (Val121 in the cyanobacterial proteins) whether or not a cross-link is present. Group I 2/2 Hb sequence alignment suggests that a valine is strongly preferred at position 121. The heme−121 interaction limits solvent access to the heme group and is expected to contribute to the stability of the fold and heme affinity. In the 3/3 fold, the H helix is straight, and the equivalent contact is provided by the residue at G5 (Supporting Information Figures S9 and S10).

Comparison of Ferric rGlbN-R and rGlbN-A. The results of the in vivo experiments indicated that GlbN-R served not only as the starting material for GlbN-A but also in some physiological capacity. It was therefore of interest to determine how these two states of the protein differed. Heme attachment does not cause major structural changes (*11*, *23*). However, the conformation of His117 and its environment may be affected by the post-translational modification. To identify spectral conditions favorable to local structure characterization, a pH titration was performed at 25 °C. His117 CδH and CεH ^{1}H resonances were followed as the pH* of an rGlbN-R solution was varied (Supporting Information Figure S11). The signals were sharpest at basic pH, and precipitation was observed below pH 5.8. Fitting the chemical shift data to a Henderson−Hasselbalch equation adapted for NMR titrations (*27*) returned an apparent pK_a of 6.15 ± 0.05 (estimated uncertainty) and a Hill coefficient of unity in agreement with a single ionization event. The pK_a value is lower than that measured in *Synechocystis* 6803 rGlbN-R (6.9 (*7*)), and this property may be related to the enhanced propensity of cross-link formation in *Synechococcus* 7002 rGlbN-R at neutral pH.

NOE data were collected at pH ~7.8 to ensure sharp lines and a high population of His117 in the neutral state. Under those conditions, the rotameric state of the residue (χ_1 angle) was $g-$, in contrast to the *t* state imposed by the linkage to the heme group. NOEs were detected from the imidazole ring to Ile111 (Supporting Information Figure S12) but none to the heme group. These NOEs, along with several NOEs involving nearby residues, persisted at neutral pH and were used to model the environment of His117. Figure 6 illustrates the average conformation compatible with the observed dipolar contacts in that region of the protein: His117 is not poised for reaction. However, only a ~60° χ_1 rotation appeared necessary to bring the imidazole ring in contact with the heme 2-vinyl.

In Vitro Peroxidase Activity of rGlbN. The elevated ROS/RNS levels in Δ*glbN Synechococcus* 7002 cells suggested a participation of GlbN in eliminating these species. The structure

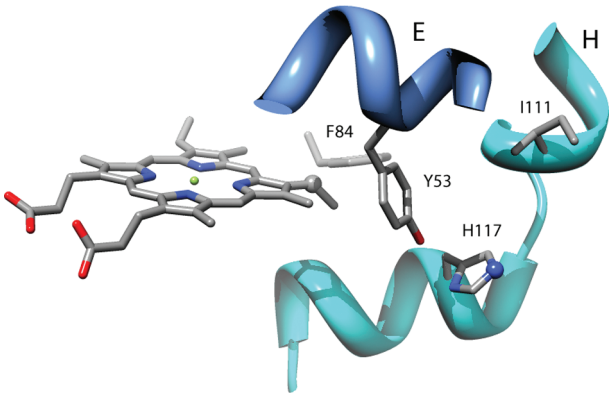

FIGURE 6: The environment of His117 in wild-type *Synechococcus* 7002 rGlbN-R. Portions of the E and H helix are shown with ribbons. The atoms bonded in rGlbN-A (CAB of the *b* heme and NE2 of His117) are represented with spheres.

of rGlbN presented the proximal histidine as engaged in the classical hemoglobin H-bond interaction (here, His70 NδH−Met66 O) rather than a peroxidase-like His NδH−Asp Oγ interaction (*46*). However, accessibility of the heme iron and hydrogen-bonding residues on the distal side (Tyr B10 and Gln E7, which are available to interact with exogenous ligand (*2*)) could favor the chemistry. Furthermore, the ^{15}N chemical shift of C^{15}N$^-$ bound to H117A *Synechococcus* 7002 rGlbN (a model for rGlbN-R) indicates a heme electronic distribution closer to that of horseradish peroxidase than of typical globins (*8*). The peroxidase activity of non-cross-linked and cross-linked rGlbNs was therefore examined in vitro. H_2O_2, a common ROS generated in cyanobacterial O_2 metabolism, was chosen as the peroxide and guaiacol as the external reductant to allow comparison with the documented pseudoperoxidase activities of Hbs from *Oryza sativa* (*47*) and *Arabidopsis thaliana* (*48*).

Figure 7 shows the results of rGlbN-R and rGlbN-A catalyzed oxidation of guaiacol at constant ~10^4-fold excess of guaiacol to protein. The observed activity was linearly dependent on the concentration of rGlbN (0.65−4.5 μM) and was inhibited by the presence of CN$^-$. The rise in product concentration was linear only over a short time (~0.5−5 min), an observation that could not be explained through the consumption of substrate and instead reflected rapid Hb deactivation due to heme damage evidenced by a decrease in the absorbance at the Soret maximum. Heme damage was aggravated when His46 was replaced with a leucine, suggesting a protective role for the *bis*-histidine configuration (data not shown). Leaving aside this limitation, the initial velocity for Hb-catalyzed guaiacol oxidation obeyed classical Michaelis−Menten kinetics. The catalytic efficiency (k_{cat}/K_M) for rGlbN-R and rGlbN-A was approximately 2 and 3 M^{-1} s^{-1}, respectively, or 100-fold lower than rice Hb (pH 6.0), 10^5-fold lower than horseradish peroxidase (pH 6.0) (*47*), and 10^4-fold lower than lignin peroxidase (pH 3.5) (*49*). Thus, rGlbN exhibited negligible peroxidase activity in the guaiacol assay.

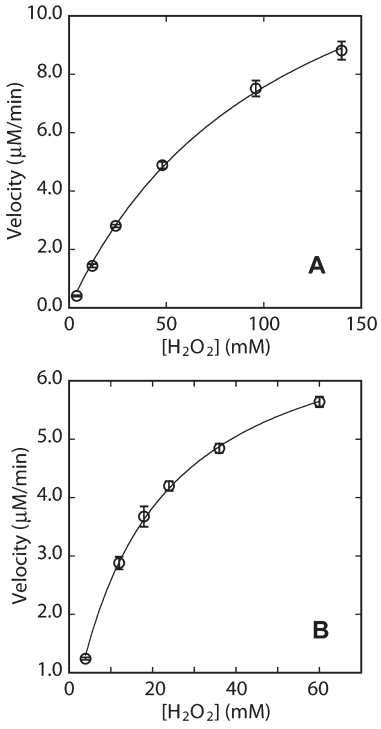

FIGURE 7: Peroxidase activity of wild-type *Synechococcus* 7002 rGlbN in the (A) rGlbN-R state and (B) rGlbN-A state. The protein concentrations were 1.3 μM (A) and 2.1 μM (B). Other conditions were room temperature, pH 7.3, and 10 mM guaiacol. Each point corresponds to triplicate initial velocity measurements. The lines illustrate the fit to the Michaelis−Menten equation. Kinetic parameters were (A) $K_M = 111 \pm 9$ mM and $k_{cat} = (2.05 \pm 0.10) \times 10^{-1}$ s^{-1} and (B) $K_M = 18.8 \pm 0.7$ mM and $k_{cat} = (5.88 \pm 0.08) \times 10^{-2}$ s^{-1}.

DISCUSSION

The *glbN* gene of *Synechococcus* 7002 is likely constitutively expressed, and GlbN is nonessential under standard growth conditions. Moreover, proteomic analyses indicate that GlbN is not synthesized at high levels. Collectively, these observations are consistent with a catalytic function for GlbN instead of simple ligand binding. As detected by the fluorescent tracer CM-H_2DCFDA, the Δ*glbN* mutant cells accumulate higher levels of ROS/RNS than wild-type cells grown under standard conditions and under NO challenge. These clues prompted us to perform physiological experiments to test the ability of the Δ*glbN* mutant to grow on nitrite or very high levels of nitrate. The accumulation of ROS/RNS was especially pronounced when the Δ*glbN* mutant cells were exposed to nitrite or high nitrate concentrations. The low in vitro peroxidase activity of the protein showed that GlbN was unlikely to eliminate ROS and strongly suggested that GlbN plays a role in protecting against RNS, specifically peroxynitrite.

Plant nitrate reductases utilize a molybdopterin cofactor to catalyze the production of nitrite from nitrate. When acting on nitrite, these enzymes generate NO and, under aerobic conditions, superoxide anions, which combine with NO to form peroxynitrite (*50*, *51*). NO production from nitrite has also been reported in the cyanobacterium *Synechococcus leopoliensis* (*S. elongatus* PCC 6301, UTEX B 625), a side reaction related to the activity of NarB, the assimilatory, ferredoxin-dependent nitrate reductase, which contains the same Mo-containing cofactor as the plant enzymes (*52*). Therefore, it is likely that *Synechococcus* 7002 NarB will similarly be responsible for the generation of RNS. Nitrite reductase (NirA), the next enzyme in the pathway of nitrate assimilation, reduces nitrite via NO as an intermediate (*53*), and adventitious release of NO by this enzyme could also contribute to peroxynitrite accumulation in cells grown on nitrate or nitrite. Although we cannot at this time rule out the possibility that GlbN directly protects cells from NO, we currently favor the hypothesis that its principal activity is protection from peroxynitrite because the Δ*glbN* mutant was more sensitive than wild type to high nitrate concentrations under fully oxic growth conditions.

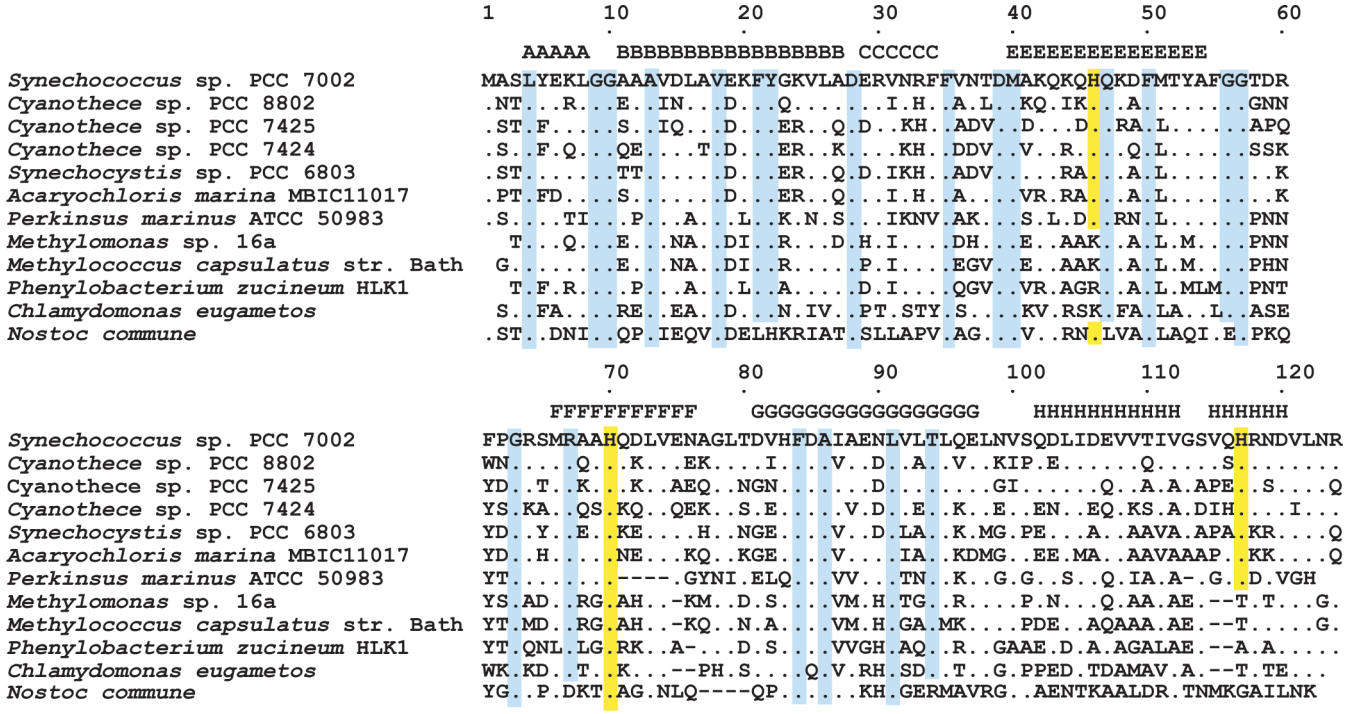

FIGURE 8: Alignment of 10 Group I 2/2 Hb sequences closely related to *Synechococcus* 7002 GlbN: *Synechococcus* sp. PCC 7002 (gi170078229|YP_001734867.1; 1−124); *Cyanothece* sp. PCC 8802 (gi257058098|YP_003135986; 70% identity; 1−124); *Cyanothece* sp. PCC 7425 (gi196239073|YP_002484366.1; 62%; 1−124); *Cyanothece* sp. PCC 7424 (gi218442058|YP_002380387.1; 58%; 1−124); *Synechocystis* sp. PCC 6803 (gi16330583|NP_441311.1; 59%; 1−124); *A. marina* MBIC11017 (gi158333678|YP_001514850.1; 59%; 1−124); *P. marinus* ATCC 50983 (gi239893688|EER13985.1; 56%; 1−116); *Methylomonas* sp. 16[a] (gi112383422|gb|ABI17848.1; 55%; 7−122); *Methylococcus capsulatus* str. Bath (gi53803300|YP_114918.1; 54%; 15−131); *Phenylobacterium zucineum* HLK1 (gi197106697|YP_002132074.1; 50%; 18−133); and *C. eugametos* globin LI637 (gi1707907|sp|Q08753.1; 46%; 43−158). The top line indicates helical regions. Residues conserved among the 11 proteins are set on a blue background. The sequence of *N. commune* GlbN (gi232163|Q00812; 30%; 1−119), though more distant, is included for reference. The three histidines discussed in the text are set on a yellow background. His70 (proximal) is the only strictly conserved residue in the superfamily.

Precedents for reactions with peroxynitrite and NO exist among globins. NO detoxification activity has been reported for *M. bovis* HbN (*39*) and is compatible with hexacoordination and other globin structural properties (*54*, *55*); it is further supported by the resemblance between the structure of *Synechococcus* 7002 GlbN and that of *Synechocystis* 6803 GlbN, whose reactivity toward NO was discussed by Hargrove and co-workers (*54*). Under certain conditions, globins are also capable of converting peroxynitrite into nitrate (*56*). If GlbN functions as a nitroxylase or a dioxygenase, nitrate formation would result in a ferric heme that would have to be reduced for turnover to occur. Cyanobacteria contain an abundant pool of reduced ferredoxin that is likely to be adequate for this purpose.

Two specific structural features of *Synechococcus* 7002 GlbN, *bis*-histidine coordination in the "resting state" and heme−protein cross-link, can be reexamined in the light of the new functional data. GlbN was found to operate under a broad range of conditions, including oxidative stress. Blocking the sixth coordination site of the iron with an axial histidine provides resistance to oxidative damage in neuroglobin (*57*) and α-hemoglobin in complex with the chaperone α-hemoglobin-stabilizing protein (*58*). Protection against H_2O_2-induced heme degradation is also observed in GlbN when the distal site is occupied by His46 or a strong ligand. A second role is conceivable for the *bis*-histidine configuration. When the distal histidine of *Synechococcus* 7002 GlbN is displaced by ligands such as O_2 and CO in the ferrous state and cyanide in the ferric state (*6*), His46 moves away from the bound exogenous ligand while a large amplitude rearrangement of the B and E helices occurs (*8*). [This is illustrated with *Synechocystis* 6803 GlbN structures (*45*) in Supporting Information Figure S7.] Although no binding partner has yet been identified, conformational changes upon distal ligand replacement might additionally signal that RNS processing is taking place.

A significant portion of the protein extracted from the cyanobacterial cells grown under microoxic conditions appeared to contain high levels of the heme−protein cross-link, whereas lower levels of cross-linked heme were observed in GlbN extracted from cells grown under normal oxic conditions. The structural model revealed that unreacted His117 points preferentially toward the solvent rather than toward the heme and that the protein is otherwise minimally perturbed by the post-translational modification. However, it is interesting to note that binding of NO can weaken the proximal histidine−Fe bond (*59*) and lower heme affinity. If the function of GlbN requires it to coordinate NO to the iron (e.g., for O_2 nitroxylation under microoxic conditions (*60*)), formation of the heme−protein cross-link could serve to prevent heme loss. Protection against NO challenge was also observed under standard oxic conditions, which do not fully promote the formation of the cross-link. Under this condition, NO dioxygenation is expected to occur. The dioxygenation mechanism involves binding of O_2 to the iron (*61*), which would not be as detrimental to the integrity of the holoprotein.

Histidine−heme cross-links of the Nε2−vinyl Cα type have been reported only in *Synechocystis* 6803 and *Synechococcus* 7002 GlbNs. Cysteine−heme cross-links of the Sγ−vinyl Cα type are found in *c* cytochromes and are therefore quite common. The in vivo observations in *Synechococcus* 7002 suggest that the redox status of the cell, along with the absence of dioxygen, prompts the

post-translational heme modification. It is possible that a histidine is better suited to the task and in-cell conditions than the thiol group of cysteine, perhaps because the latter could undergo undesired S-nitrosylation.

Conditional formation of the cross-link suggests yet another hypothesis. When O_2 is available, GlbN that contains *b* heme undergoes slow post-translational modification. When O_2 levels drop, the cross-link is made, immobilizing heme in the protein matrix and rendering it unavailable for catabolism into the linear tetrapyrrole products necessary for assembly of phycobiliproteins (*62*). Covalent modification of GlbN by heme is therefore a sensor of the cellular oxygen status, and GlbN could play an important regulatory role as a secondary signaling molecule through binding interactions with a transcription factor, sigma factor, or sensor kinase.

Figure 8 presents the primary structure alignment for ten Group I 2/2 Hbs closely related to *Synechococcus* 7002 GlbN. The identity levels range from 70% (*Cyanothece* 8802) to 46% (*C. eugametos*). The *Cyanothece* 8802, *Acaryochloris marina*, and *Perkinsus marinus* GlbNs contain histidines at positions 46 and 117; they are likely to exhibit *bis*-histidine coordination in the resting state and to be capable of post-translational heme modification. These GlbNs may have a function related to that proposed for *Synechococcus* 7002 GlbN. The absence of His46 and His117 in other Group I proteins suggests different GlbN roles or different cellular conditions for activity. The more distant *N. commune* GlbN (Figure 8, last sequence, 30% identity) is thought to be a dioxygen scavenger in vegetative *Nostoc* sp. cells under microoxic conditions and in heterocysts (*15*), specialized cells whose function in nitrogen fixation is critically dependent on the absence of oxygen. The different nitrogen metabolism pathway, low sequence identity, and mixed report of endogenous hexacoordination (*13*, *14*) are consistent with a function distinct from that of *Synechococcus* 7002 GlbN.

As noted above, cyanobacteria may adventitiously produce NO that could form peroxynitrite when superoxide is present. Additionally, many cyanobacteria that have the *glbN* gene are soil organisms, and these bacteria may be associated with organisms that produce NO as a result of anaerobic respiration using nitrate as an electron acceptor (denitrification). Many cyanobacteria encounter anoxic conditions daily at night, when fermentative metabolism is common, and these conditions would also promote denitrification by associated bacteria. Further in vivo and in vitro studies of *Synechococcus* 7002 and other cyanobacterial GlbNs will refine functional hypotheses involving nitrate, nitric oxide, and peroxynitrite, as well as novel structure−activity relationships in the Hb superfamily.

ACKNOWLEDGMENT

Figure 5 was prepared with Molscript (*63*). The authors thank Drs. Craig Praul and Deborah Grove of the Genomics Core Facility (Huck Institutes of the Life Sciences, University Park) for assistance and advice in transcription profiling by SOLiD and in the initial reverse-transcription experiments, respectively.

SUPPORTING INFORMATION AVAILABLE

Summaries of growth and RT-PCR procedures, protein preparation for NMR experiments, low-temperature fluorescence data, and NMR structure determination; heme structure and nomenclature in GlbN-R and GlbN-A (Figure S1); construction of the Δ*glbN* mutant (Figure S2); doubling times (Table S1); low-temperature fluorescence data (Figure S3); optical spectra of heterologously produced rGlbNs (Figure S4); photographs of cell cultures (Figure S5); comparison of the transcriptional levels (Table S2); electronic absorption spectrum of a liquid culture of *E. coli* cells overproducing GlbN (Figure S6); heme environment in ferric *Synechocystis* 6803 and *Synechococcus* 7002 rGlbN-As (Figure S7); tunnels in the GlbN-A structure (Figure S8); comparison of heme/C-terminal interactions in rGlbN-A and myoglobin (Figure S9); G helix in rGlbN-A (Figure S10); NMR pH titration of His117 in rGlbN-R (Figure S11); NOEs defining the environment of His117 in rGlbN-R (Figure S12). This material is available free of charge via the Internet at http://pubs.acs.org.

REFERENCES

1. Vinogradov, S. N., Hoogewijs, D., Bailly, X., Arredondo-Peter, R., Guertin, M., Gough, J., Dewilde, S., Moens, L., and Vanfleteren, J. R. (2005) Three globin lineages belonging to two structural classes in genomes from the three kingdoms of life. *Proc. Natl. Acad. Sci. U.S.A. 102*, 11385–11389.
2. Pesce, A., Couture, M., Dewilde, S., Guertin, M., Yamauchi, K., Ascenzi, P., Moens, L., and Bolognesi, M. (2000) A novel two-over-two α-helical sandwich fold is characteristic of the truncated hemoglobin family. *EMBO J. 19*, 2424–2434.
3. Vuletich, D. A., and Lecomte, J. T. J. (2006) A phylogenetic and structural analysis of truncated hemoglobins. *J. Mol. Evol. 62*, 196–210.
4. Vinogradov, S. N., and Moens, L. (2008) Diversity of globin function: enzymatic, transport, storage, and sensing. *J. Biol. Chem. 283*, 8773–8777.
5. Nicoletti, F. P., Comandini, A., Bonamore, A., Boechi, L., Boubeta, F. M., Feis, A., Smulevich, G., and Boffi, A. (2010) Sulfide binding properties of truncated hemoglobins. *Biochemistry 49*, 2269–2278.
6. Scott, N. L., Falzone, C. J., Vuletich, D. A., Zhao, J., Bryant, D. A., and Lecomte, J. T. J. (2002) The hemoglobin of the cyanobacterium *Synechococcus* sp. PCC 7002: evidence for hexacoordination and covalent adduct formation in the ferric recombinant protein. *Biochemistry 41*, 6902–6910.
7. Vu, B. C., Vuletich, D. A., Kuriakose, S. A., Falzone, C. J., and Lecomte, J. T. J. (2004) Characterization of the heme-histidine cross-link in cyanobacterial hemoglobins from *Synechocystis* sp. PCC 6803 and *Synechococcus* sp. PCC 7002. *J. Biol. Inorg. Chem. 9*, 183–194.
8. Vu, B. C., Nothnagel, H. J., Vuletich, D. A., Falzone, C. J., and Lecomte, J. T. J. (2004) Cyanide binding to hexacoordinate cyanobacterial hemoglobins: Hydrogen bonding network and heme pocket rearrangement in ferric H117A *Synechocystis* Hb. *Biochemistry 43*, 12622–12633.
9. Couture, M., Das, T. K., Savard, P. Y., Ouellet, Y., Wittenberg, J. B., Wittenberg, B. A., Rousseau, D. L., and Guertin, M. (2000) Structural investigations of the hemoglobin of the cyanobacterium *Synechocystis* PCC 6803 reveal a unique distal heme pocket. *Eur. J. Biochem. 267*, 4770–4780.
10. Scott, N. L., and Lecomte, J. T. J. (2000) Cloning, expression, purification, and preliminary characterization of a putative hemoglobin from the cyanobacterium *Synechocystis* sp. PCC 6803. *Protein Sci. 9*, 587–597.
11. Vuletich, D. A., Falzone, C. J., and Lecomte, J. T. J. (2006) Structural and dynamic repercussions of heme binding and heme-protein cross-linking in *Synechococcus* sp. PCC 7002 hemoglobin. *Biochemistry 45*, 14075–14084.
12. Potts, M., Angeloni, S. V., Ebel, R. E., and Bassam, D. (1992) Myoglobin in a cyanobacterium. *Science 256*, 1690–1691.
13. Thorsteinsson, M. V., Bevan, D. R., Ebel, R. E., Weber, R. E., and Potts, M. (1996) Spectroscopical and functional characterization of the hemoglobin of *Nostoc commune* UTEX 584 (Cyanobacteria). *Biochim. Biophys. Acta 1292*, 133–139.
14. Thorsteinsson, M. V., Bevan, D. R., Potts, M., Dou, Y., Eich, R. F., Hargrove, M. S., Gibson, Q. H., and Olson, J. S. (1999) A cyanobacterial hemoglobin with unusual ligand binding kinetics and stability properties. *Biochemistry 38*, 2117–2126.
15. Hill, D. R., Belbin, T. J., Thorsteinsson, M. V., Bassam, D., Brass, S., Ernst, A., Boger, P., Paerl, H., Mulligan, M. E., and Potts, M. (1996) GlbN (cyanoglobin) is a peripheral membrane protein that is restricted to certain *Nostoc* spp. *J. Bacteriol. 178*, 6587–6598.
16. Stevens, S. E. J., Patterson, C. O. P., and Myers, J. K. (1973) The production of hydrogen peroxide by blue-green algae: a survey. *J. Phycol. 9*, 427–430.

17. Xu, Y., Alvey, R., Byrne, P. O., Graham, J. E., Shen, G., and Bryant, D. A. (2010) Expression of genes in cyanobacteria: adaptation of endogenous plasmids as platforms for high-level gene expression in *Synechococcus* sp. PCC 7002, in Photosynthesis Research Protocols (Carpentier, R., Ed.) Humana Press, Totowa, NJ, in press.
18. Shen, G., Saunée, N. A., Williams, S. R., Gallo, E. F., Schluchter, W. M., and Bryant, D. A. (2006) Identification and characterization of a new class of bilin lyase: the *cpcT* gene encodes a bilin lyase responsible for attachment of phycocyanobilin to Cys-153 on the β-subunit of phycocyanin in *Synechococcus* sp. PCC 7002. *J. Biol. Chem. 281*, 17768–17778.
19. Li, H., and Durbin, R. (2009) Fast and accurate short read alignment with Burrows-Wheeler transform. *Bioinformatics 25*, 1754–1760.
20. Shen, G. Z., and Bryant, D. A. (1995) Characterization of a *Synechococcus* sp. strain PCC 7002 mutant lacking photosystem I. Protein assembly and energy-distribution in the absence of the photosystem I reaction-center core complex. *Photosynth. Res. 44*, 41–53.
21. Thomas, P. E., Ryan, D., and Levin, W. (1976) An improved staining procedure for the detection of the peroxidase activity of cytochrome P-450 on sodium dodecyl sulfate polyacrylamide gels. *Anal. Biochem. 75*, 168–176.
22. Chance, B., and Maehley, A. C. (1955) Assay of catalase and peroxidases. *Methods Enzymol. 2*, 764–775.
23. Pond, M. P., Vuletich, D. A., Falzone, C. J., Majumdar, A., and Lecomte, J. T. J. (2009) ^{1}H, ^{15}N, and ^{13}C resonance assignments of the 2/2 hemoglobin from the cyanobacterium *Synechococcus* sp. PCC 7002 in the ferric bis-histidine state. *Biomol. NMR Assign. 3*, 211–214.
24. Vuister, G., and Bax, A. (1993) Quantitative J correlation: a new approach for measuring three-bond $J(H^{N}H^{\alpha})$ coupling constants in ^{15}N-enriched proteins. *J. Am. Chem. Soc. 115*, 7772–7777.
25. Delaglio, F., Grzesiek, S., Vuister, G. W., Zhu, G., Pfeifer, J., and Bax, A. (1995) NMRPipe: a multidimensional spectral processing system based on UNIX pipes. *J. Biomol. NMR 6*, 277–293.
26. Goddard, T. D., and Kneller, D. G. (2006) SPARKY 3, University of California, San Francisco.
27. Markley, J. (1975) Observation of histidine residues in proteins by means of nuclear magnetic resonance spectroscopy. *Acc. Chem. Res. 8*, 70–80.
28. Pettersen, E. F., Goddard, T. D., Huang, C. C., Couch, G. S., Greenblatt, D. M., Meng, E. C., and Ferrin, T. E. (2004) UCSF Chimera—a visualization system for exploratory research and analysis. *J. Comput. Chem. 25*, 1605–1612.
29. Shen, Y., Delaglio, F., Cornilescu, G., and Bax, A. (2009) TALOS+: a hybrid method for predicting protein backbone torsion angles from NMR chemical shifts. *J. Biomol. NMR 44*, 213–223.
30. Schwieters, C. D., Kuszewski, J. J., and Clore, G. M. (2006) Using Xplor-NIH for NMR molecular structure determination. *Prog. NMR Spectrosc. 48*, 47–62.
31. (2009) CRC Handbook of Chemistry and Physics, 90th ed., CRC Press, Boca Raton, FL.
32. Kuszewski, J., and Clore, G. M. (2000) Sources of and solutions to problems in the refinement of protein NMR structures against torsion angle potentials of mean force. *J. Magn. Reson. 146*, 249–254.
33. Falzone, C. J., Vu, B. C., Scott, N. L., and Lecomte, J. T. J. (2002) The solution structure of the recombinant hemoglobin from the cyanobacterium *Synechocystis* sp. PCC 6803 in its hemichrome state. *J. Mol. Biol. 324*, 1015–1029.
34. Laskowski, R. A., Rullmannn, J. A., MacArthur, M. W., Kaptein, R., and Thornton, J. M. (1996) AQUA and PROCHECK-NMR: programs for checking the quality of protein structures solved by NMR. *J. Biomol. NMR 8*, 477–486.
35. Vriend, G., and Sander, C. (1993) Quality control of protein models: directional atomic contact analysis. *J. Appl. Crystallogr. 26*, 47–60.
36. Petrek, M., Kosinova, P., Koca, J., and Otyepka, M. (2007) MOLE: a Voronoi diagram-based explorer of molecular channels, pores, and tunnels. *Structure 15*, 1357–1363.
37. Funk, C., and Vermaas, W. (1999) A cyanobacterial gene family coding for single-helix proteins resembling part of the light-harvesting proteins from higher plants. *Biochemistry 38*, 9397–9404.
38. Barber, J., Nield, J., Duncan, J., and Bibby, T. S. (2006) Accessory chlorophyll proteins in cyanobacterial photosystem I, in Photosystem I: The Light-Driven Plastocyanin:Ferredoxin Oxidoreductase (Golbeck, J. H., Ed.) pp 99−117, Springer, Dordrecht, The Netherlands.
39. Ouellet, H., Ouellet, Y., Richard, C., Labarre, M., Wittenberg, B., Wittenberg, J., and Guertin, M. (2002) Truncated hemoglobin HbN protects *Mycobacterium bovis* from nitric oxide. *Proc. Natl. Acad. Sci. U.S.A. 99*, 5902–5907.
40. Ferrer-Sueta, G., and Radi, R. (2009) Chemical biology of peroxynitrite: kinetics, diffusion, and radicals. *ACS Chem. Biol. 4*, 161–177.
41. Nardini, M., Pesce, A., Milani, M., and Bolognesi, M. (2007) Protein fold and structure in the truncated (2/2) globin family. *Gene 398*, 2–11.
42. Hoy, J. A., Kundu, S., Trent, J. T., III, Ramaswamy, S., and Hargrove, M. S. (2004) The crystal structure of *Synechocystis* hemoglobin with a covalent heme linkage. *J. Biol. Chem. 279*, 16535–16542.
43. Pesce, A., Milani, M., Nardini, M., and Bolognesi, M. (2008) Mapping heme-ligand tunnels in group I truncated(2/2) hemoglobins. *Methods Enzymol. 436*, 303–315.
44. Daigle, R., Guertin, M., and Lagüe, P. (2009) Structural characterization of the tunnels of *Mycobacterium tuberculosis* truncated hemoglobin N from molecular dynamics simulations. *Proteins 75*, 735–747.
45. Trent, J. T., III, Kundu, S., Hoy, J. A., and Hargrove, M. S. (2004) Crystallographic analysis of synechocystis cyanoglobin reveals the structural changes accompanying ligand binding in a hexacoordinate hemoglobin. *J. Mol. Biol. 341*, 1097–1108.
46. Poulos, T. L. (1996) The role of the proximal ligand in heme enzymes. *J. Biol. Inorg. Chem. 1*, 356–359.
47. Violante-Mota, F., Tellechea, E., Moran, J. F., Sarath, G., and Arredondo-Peter, R. (2010) Analysis of peroxidase activity of rice (*Oryza sativa*) recombinant hemoglobin 1: implications for in vivo function of hexacoordinate non-symbiotic hemoglobins in plants. *Phytochemistry 71*, 21–26.
48. Sakamoto, A., Sakurao, S. H., Fukunaga, K., Matsubara, T., Ueda-Hashimoto, M., Tsukamoto, S., Takahashi, M., and Morikawa, H. (2004) Three distinct *Arabidopsis* hemoglobins exhibit peroxidase-like activity and differentially mediate nitrite-dependent protein nitration. *FEBS Lett. 572*, 27–32.
49. Koduri, R. S., and Tien, M. (1995) Oxidation of guaiacol by lignin peroxidase. Role of veratryl alcohol. *J. Biol. Chem. 270*, 22254–22258.
50. Yamasaki, H., and Sakihama, Y. (2000) Simultaneous production of nitric oxide and peroxynitrite by plant nitrate reductase: in vitro evidence for the NR-dependent formation of active nitrogen species. *FEBS Lett. 468*, 89–92.
51. Moreau, M., Lindermayr, C., Durner, J., and Klessig, D. F. (2010) NO synthesis and signaling in plants—where do we stand? *Physiol. Plant. 138*, 372–383.
52. Mallick, N., Rai, L. C., Mohn, F. H., and Soeder, C. J. (1999) Studies on nitric oxide (NO) formation by the green alga *Scenedesmus obliquus* and the diazotrophic cyanobacterium *Anabaena doliolum*. *Chemosphere 39*, 1601–1610.
53. Kuznetsova, S., Knaff, D. B., Hirasawa, M., Lagoutte, B., and Sétif, P. (2004) Mechanism of spinach chloroplast ferredoxin-dependent nitrite reductase: spectroscopic evidence for intermediate states. *Biochemistry 43*, 510–517.
54. Smagghe, B. J., Trent, J. T., III, and Hargrove, M. S. (2008) NO dioxygenase activity in hemoglobins is ubiquitous in vitro, but limited by reduction in vivo. *PLoS ONE 3*, e2039.
55. Gardner, P. R. (2005) Nitric oxide dioxygenase function and mechanism of flavohemoglobin, hemoglobin, myoglobin and their associated reductases. *J. Inorg. Biochem. 99*, 247–266.
56. De Marinis, E., Casella, L., Ciaccio, C., Coletta, M., Visca, P., and Ascenzi, P. (2009) Catalytic peroxidation of nitrogen monoxide and peroxynitrite by globins. *IUBMB Life 61*, 62–73.
57. Lardinois, O. M., Tomer, K. B., Mason, R. P., and Deterding, L. J. (2008) Identification of protein radicals formed in the human neuroglobin-H_2O_2 reaction using immuno-spin trapping and mass spectrometry. *Biochemistry 47*, 10440–10448.
58. Hamdane, D., Vasseur-Godbillon, C., Baudin-Creuza, V., Hoa, G. H., and Marden, M. C. (2007) Reversible hexacoordination of α-hemoglobin-stabilizing protein (AHSP)/α-hemoglobin versus pressure. Evidence for protection of the α-chains by their chaperone. *J. Biol. Chem. 282*, 6398–6404.
59. Traylor, T. G., and Sharma, V. S. (1992) Why NO? *Biochemistry 31*, 2847–2849.
60. Angelo, M., Hausladen, A., Singel, D. J., and Stamler, J. S. (2008) Interactions of NO with hemoglobin: from microbes to man. *Methods Enzymol. 436*, 131–168.
61. Gardner, P. R., Gardner, A. M., Brashear, W. T., Suzuki, T., Hvitved, A. N., Setchell, K. D., and Olson, J. S. (2006) Hemoglobins dioxygenate nitric oxide with high fidelity. *J. Inorg. Biochem. 100*, 542–550.
62. Schluchter, W. M., Shen, G., Alvey, R. M., Biswas, A., Saunée, N. A., Williams, S. R., Miller, C. A., and Bryant, D. A. (2010) Phycobiliprotein biosynthesis in cyanobacteria: structure and function of enzymes involved in post-translational modification, in Recent Advances in Phototrophic Prokaryotes (Advances in Experimental Medicine & Biology) (Hallenbeck, P. C., Ed.) Springer, Berlin.
63. Kraulis, P. (1991) MOLSCRIPT: a program to produce both detailed and schematic plots of protein structures. *J. Appl. Crystallogr. 24*, 946–950.